

# Phase-transitions induced by easy-plane anisotropy in the classical Heisenberg antiferromagnet on a triangular lattice: a Monte Carlo simulation

Luca Capriotti\*

*Dipartimento di Fisica dell'Università di Firenze and Istituto Nazionale di Fisica della Materia (INFM),  
Largo E. Fermi 2, I-50125 Firenze, Italy,  
and Scuola Internazionale Superiore di Studi Avanzati, via Beirut 2-4, 34013 Trieste, Italy*

Ruggero Vaia†

*Istituto di Elettronica Quantistica del Consiglio Nazionale delle Ricerche, via Panciatichi 56/30, I-50127 Firenze, Italy,  
and Istituto Nazionale di Fisica della Materia (INFM).*

Alessandro Cuccoli‡, Valerio Tognetti§

*Dipartimento di Fisica dell'Università di Firenze and Istituto Nazionale di Fisica della Materia (INFM),  
Largo E. Fermi 2, I-50125 Firenze, Italy  
(December 2, 2024)*

We present the results of Monte Carlo simulations for the antiferromagnetic classical XXZ model with easy-plane exchange anisotropy on the triangular lattice, which causes frustration of the spin alignment. The behaviour of this system is similar to that of the antiferromagnetic XY model on the same lattice, showing the signature of a Berezinskii-Kosterlitz-Thouless transition, associated to vortex-antivortex unbinding, and of an Ising-like one due to the chirality, the latter occurring at a slightly higher temperature. Data for internal energy, specific heat, magnetic susceptibility, correlation length, and some properties associated with the chirality are reported in a broad temperature range, for lattice sizes ranging from  $24 \times 24$  to  $120 \times 120$ ; four values of the easy-plane anisotropy are considered. Moving from the strongest towards the weakest anisotropy (1%) the thermodynamic quantities tend to the isotropic model behaviour, and the two transition temperatures decrease by about 25 % and 22 %, respectively.

## I. INTRODUCTION

The critical behaviour of classical two-dimensional (2D) frustrated models has raised the interest of several scientists in the last years. Popular realization of such models are Heisenberg<sup>1,2,3</sup> and the XY<sup>4,5</sup> antiferromagnet on a triangular lattice, as well as the fully frustrated XY model on the square lattice<sup>6,7</sup>; the role of frustration shows up in the particular nature of the order parameter in the first one, and in the presence of two kinds of symmetry in the other two. In the triangular-lattice models the minimum energy configuration (say, the ground state) is a ferromagnetic arrangement of the spins in each of three sublattices, with a relative rotation of  $120^\circ$  between each other. The three vertices of each lattice plaquette belong to different sublattices, and it is possible to associate to each plaquette a vector, the chirality, that defines the rotation of the spin direction around the plaquette. In the XY case the (staggered) chirality turns into a scalar order parameter whose sign distinguishes between two degenerate ground states.

In this paper we consider the XXZ triangular antiferromagnet (TAF), a system that shares the symmetry of the XY model and is a more realistic description of a spin system. In addition, to treat three-dimensional spins is a necessary step for studying the corresponding quantum system by means of the pure-quantum self-consistent harmonic approximation<sup>8,9,10,11</sup>. In the XXZ TAF the easy-plane anisotropy results in a double degeneracy of the ground state. This model is thus expected to belong to the universality class of the frustrated XY model. A

very fascinating aspect of the thermodynamics of such a system is that it has two order parameters, the (in-plane) magnetization and the chirality, with two distinct symmetry groups, continuous  $SO(2)$  rotations and discrete  $Z_2$  lattice reflections, respectively. This has surprising consequences in view of Mermin-Wagner's theorem<sup>12</sup>, that can be applied only in the first case to infer that the magnetization must vanish at any nonzero temperature, according to the expected Berezinskii-Kosterlitz-Thouless (BKT)<sup>13</sup> critical behaviour associated with the rotation symmetry in the  $xy$  plane, while long-range order and an Ising-like phase transition are allowed for the chirality. This rich structure was observed in Monte Carlo (MC) simulations for the XY model. However, it was not clear whether the two transitions are distinct, with an intermediate phase, or they are manifestations of a new universality class, in which the two transition temperatures could be molten in a single multicritical point: from early numerical simulations<sup>4,5</sup> they turned out to be weakly different, but in view of their uncertainty no firm conclusions could be inferred. Very recently, high-precision MC studies of the XY TAF model and of its Villain version were reported by Olsson<sup>7</sup>, who established that the BKT transition occurs at a temperature  $\sim 1\text{--}1.4\%$  lower than the Ising-like one.

Qualitatively, the results we find for the XXZ TAF are rather similar to those already known for the XY TAF, for any anisotropy strength considered, even close to the isotropic limit. The observed changes reflect the enhanced spin fluctuations out from the easy plane and the crossover towards the isotropic limit. The features of

both the Ising-like and the BKT transition shift to lower temperatures. Although the numerical uncertainty is not much smaller than their difference, from our simulations the BKT critical temperature turns out slightly smaller than the other one, systematically for all anisotropy values.

In Sec. II we introduce the XXZ model and its ground state, discussing the connections with the corresponding XY model and its critical behaviour. In Sec. III the MC simulation algorithm is described and the definitions of the calculated thermodynamic quantities are given. Eventually, in Sec. IV the MC results are reported, generally for four different values of the anisotropy constant, and analyzed for their critical behaviour and the finite-size effects. Conclusions are briefly drawn in Sec. V.

## II. THE XXZ MODEL

### A. Definition of the model

We consider the classical XXZ Hamiltonian

$$\mathcal{H} = \frac{J}{2} \sum_{\mathbf{i}, \mathbf{d}} (s_{\mathbf{i}}^x s_{\mathbf{i}+\mathbf{d}}^x + s_{\mathbf{i}}^y s_{\mathbf{i}+\mathbf{d}}^y + \lambda s_{\mathbf{i}}^z s_{\mathbf{i}+\mathbf{d}}^z), \quad (1)$$

where  $J$  is the positive (antiferromagnetic) exchange constant, and  $(s_{\mathbf{i}}^x, s_{\mathbf{i}}^y, s_{\mathbf{i}}^z)$  are the Cartesian components of unitary vectors, the classical spins, sitting on the sites  $\{\mathbf{i}\}$  of a two-dimensional triangular lattice. The interaction is restricted to nearest-neighbours and  $\mathbf{d}$  runs over their relative displacements ( $|\mathbf{d}| = 1$ ). The use of unitary spin vectors produces no loss of generality in the study of a classical system since the case of generic spin  $S$  can be taken into account by rescaling the exchange constant  $J \rightarrow JS^2$ . The exchange constant sets the natural energy scale of the system: hence, in the following, energies and temperatures will be always given in units of  $J$ .

The planar character of the system is due to the presence of the constant  $\lambda \in [0, 1]$ , which weakens the interaction of the  $z$  spin components, energetically favouring configurations with the spins lying in the  $xy$  plane (easy-plane). For  $\lambda = 1$  the isotropic Heisenberg model<sup>1,3</sup> is recovered; for  $\lambda = 0$  (when the model is also known as XX0) the spin components on the  $z$  axis do not even appear in the Hamiltonian, making it formally identical to that of the XY model, which was the subject of some previous works<sup>4,5</sup>. However, in the XY and XX0 models the phase-spaces are different: in the former the spins are two-dimensional vectors, while in the latter they can fluctuate out of the  $xy$  plane. Of course the thermodynamic properties are expected to be quantitatively different in the two models.

### B. Ground state properties

The ground state configuration of (1) can be found<sup>14</sup> by minimizing the energy of any single elementary triangular cell of the lattice. In this way one gets that,

for every value of  $\lambda \in [0, 1]$ , the ground state consists of coplanar spins forming  $\pm 2\pi/3$  angles between nearest-neighbours (see Fig. 1). In contrast to the isotropic case, where the plane in which the  $2\pi/3$  structure lies can take any direction in spin space, in the XXZ model (as well as in the XY model) such structure must take place in the easy-plane. In any case this leads to a  $\sqrt{3} \times \sqrt{3}$  periodic ground state.

In the XY and XXZ unfrustrated systems, like the ferromagnet on a general lattice or the antiferromagnet on a bipartite lattice, the degeneracy of the ground state, connected to the possible equivalent choices of the direction of alignment of spins in the space, corresponds to the  $SO(2)$  symmetry group. In the planar TAF the frustration effect causes an additional two-fold degeneracy of the ground state, which is due to chirality (or helicity), defined as the sign of rotation of the spins along the sides of each elementary triangle. Since global spin rotations in the easy-plane conserve the chirality, one configuration cannot be obtained from the other one by pure rotations but it is necessary to include some other symmetry operation such as lattice reflection; i.e. the whole degeneracy corresponds to the group  $SO(2) \times Z_2$ .

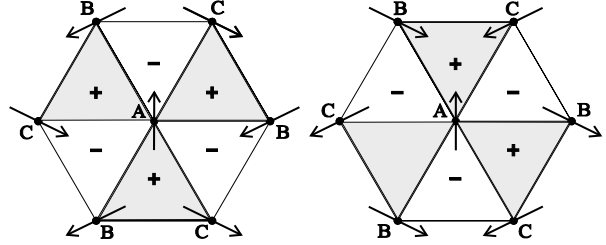


FIG. 1. Two degenerate ground states. The plus and minus denote the sign of the chirality of each elementary cell and the two configurations are characterized by opposite staggered chirality. The letters A, B and C label the three sublattices on which the spins are ferromagnetically aligned.

### C. Phase transitions

As it has been pointed out by Lee *et al.*<sup>5</sup>, the existence of the extra degeneracy of the ground state allows the 2D frustrated XY model to support, in addition to spin waves and vortices, a third type of elementary excitation associated with domain-wall formation between regions with opposite staggered chirality (solitons). The first two are responsible for the loss of orientational order with increasing temperature, while the latter causes the destruction of chirality order. Then, the thermodynamics is characterized by the interplay of these three types of elementary excitations.

The ground state of the three sublattices consists of ferromagnetically aligned spins, the interaction between those of the same sublattice being mediated by the spins of the other two. Thus the physics of the three sublattices is expected to be similar to the physics of the whole lattice in the XY unfrustrated models and a

Berezinskii-Kosterlitz-Thouless (BKT) topological transition becomes plausible<sup>13</sup>. Besides, since lattice reflection is a discrete symmetry, the system can have long range chirality order at finite temperature without violating the Mermin-Wagner theorem<sup>12</sup> and an order-disorder Ising-like transition is expected. Indeed this is the situation observed for the first time in the MC study performed by Miyashita and Shiba<sup>4</sup> for the 36-state clock model and, later, by Lee *et al.*<sup>5</sup>, on the basis of group-theoretical symmetry arguments, combined with more extensive MC simulations including somewhat larger lattices (up to  $72 \times 72$ ) and without the limitations introduced by the discrete sampling of the spin orientation. Perhaps the most striking characteristic of the phase transition is the logarithmic divergence of the specific heat, quite similar to that of the Ising model, and for this reason it was associated with the order-disorder transition of the chirality. The sharp drop with increasing temperature of the staggered chirality, the counterpart of Ising magnetization, and the divergence of the corresponding chiral susceptibility are the other main characteristics of the transition connected with the loss of chirality order. Instead, the main sign of the vortex-antivortex unbinding driven BKT transition is the divergence of the spin correlation length and susceptibility<sup>4,5</sup>. Whether the two transitions are very close but distinct, each conserving the proper critical exponents, or they melt in a single phase-transition which has both Ising and BKT character in a possible new universality class, is an open problem also shared by the other realizations of the so-called fully frustrated XY model, which are generally believed to have similar critical behaviour<sup>7</sup>.

It is well known<sup>15,16,17,18</sup> that the unfrustrated XXZ model shows the BKT transition, as the XY model, at finite temperature for every value of the anisotropy constant  $\lambda < 1$  (no matter how close to 1); in particular, for  $\lambda \rightarrow 1$ , the critical temperature is predicted to approach 0 as  $1/|\ln(1 - \lambda)|$ . The phase transition in the XXZ model is again due to vortex unbinding as in the pure XY model, even if the vortices may have different character since the spins are no longer obliged to lie in the  $xy$  plane, with the spins in the vortex core pointing preferably in the out of plane direction<sup>19</sup>. Likewise, it is at least plausible that the order-disorder transition of the chirality is also present in the frustrated XXZ model for  $\lambda < 1$ ; i.e., as far as the system shows a planar character and its ground state (the  $2\pi/3$  structure of the ground state being forced to lie in the  $xy$  plane) has the two-fold additional degeneracy.

### III. MONTE CARLO SIMULATION

#### A. Simulation algorithm and procedure

We performed standard MC simulations on triangular lattices of size  $L \times L$  (along the primitive vectors directions), containing  $N = L^2$  sites and  $2N$  elementary cells, with periodic boundary conditions.  $L$  was between

24 and 120: multiples of 3 have been chosen for  $L$  to preserve the ground-state translation symmetry. In order to reduce the MC correlation time, a combination of Metropolis<sup>20</sup> and over-relaxed algorithm was used<sup>21,22</sup>, as in previous studies of the XXZ model on the square lattice<sup>18</sup>. For any given lattice size and for any temperature, the simulation procedure was the following. An initial configuration was generated at random and then a given number, typically 10 000, of Metropolis moves (one move consists of  $N$  single-particle moves) were made in order to bring the system to a thermalized configuration; after that, the accumulation of the averages started. A sample configuration, used to update the averages of the thermodynamic quantities, was taken after  $N_O = 4$  over-relaxed moves and  $N_M = 2$  Metropolis moves, the values of  $N_O$  and  $N_M$  being a compromise between computational effort and minimization of MC correlation time. Typical runs sampled 30 000 configurations. Since to our knowledge, no data is available for the XXZ TAF model, the simulation code we developed was checked in the isotropic case, for which we got results in complete agreement with those reported in the literature<sup>1,3</sup>.

The strategy adopted to choose the lattice sizes and the temperatures during the simulations was the following. We performed a sequence of simulations for the smallest lattice size ( $L = 24$ ) with a big step in temperature, in order to get a clue about the qualitative behaviour of the various quantities and to locate, at least approximatively, the critical region. Then it has been necessary to perform various simulations in the neighbourhood of the critical temperature and for larger lattice sizes, in order to locate the transition temperatures and to evaluate the finite-size effects which strongly affect the behaviour of some thermodynamic quantities.

In the following, the symbol  $\langle Q \rangle$  will denote the MC average of a general quantity  $Q$ , defined as

$$\langle Q \rangle = \frac{1}{M} \sum_{j=1}^M Q_j , \quad (2)$$

$M$  being the total number of configurations  $j$  sampled during the simulation. The uncertainties reported in the following are statistical errors, estimated in the standard way from the quadratic fluctuations of the corresponding observable. The effects of correlations were included multiplying the pure statistical errors by  $\sqrt{2\tau}$ ,  $\tau$  being the correlation time deduced from the analysis of the sequence of the sampled data for that observable<sup>23</sup>.

#### B. Thermodynamic observables

We evaluated several thermodynamic quantities in order to observe the effects of the destruction of chirality order, such as internal energy, specific heat, chirality and its susceptibility. On the other hand, spin correlation functions, correlation length and susceptibility, were calculated to investigate the presence of a BKT transition. The internal energy per spin is defined as

$$e = \frac{\langle E \rangle}{N}, \quad (3)$$

where  $E = \mathcal{H}/J$ . The specific heat can be computed, using the relation

$$c = \frac{1}{N} \frac{\langle E^2 \rangle - \langle E \rangle^2}{t^2}, \quad (4)$$

with the reduced temperature  $t = T/J$ .

The definition of the chirality, that is the sign of rotation of spins on the elementary triangle in the ground state configuration, is usually generalized<sup>1,4</sup> to nonzero temperatures as follows:

$$\kappa_{\mathbf{r}} = \frac{2}{3\sqrt{3}} (\mathbf{s}_1 \times \mathbf{s}_2 + \mathbf{s}_2 \times \mathbf{s}_3 + \mathbf{s}_3 \times \mathbf{s}_1), \quad (5)$$

where 1,2 and 3 are the corner sites of the elementary cell centered at the dual-lattice vector  $\mathbf{r}$ , always (for both upward and downward triangles) ordered in the same way (for example, counterclockwise). Unlike the XY model where, being the spins confined in the  $xy$  plane, it has only the component along the  $z$  axis, in the XXZ model the chirality is a true vector. It is normalized to 1 for a complete  $2\pi/3$  structure, when it has only the  $z$  component that can take the values  $\pm 1$ , as the Ising spin. At any finite temperature the length of  $\kappa^z$  compared to that of the other two components gives a measure of the rigidity of the  $2\pi/3$  structure, and can be taken as the order parameter. During the simulations we calculated the staggered chirality, defined as

$$\kappa = \frac{1}{2N} \left\langle \left| \sum_{\mathbf{r}} (-)^{\mathbf{r}} \kappa_{\mathbf{r}}^z \right| \right\rangle, \quad (6)$$

where the factor  $(-)^{\mathbf{r}}$  assumes the values  $\pm 1$  for downward/upward triangles, respectively.

Also interesting is the susceptibility associated to staggered chirality along the  $z$  axis, calculated as

$$\chi_{\kappa} = \frac{1}{4N} \left[ \left\langle \left| \sum_{\mathbf{r}} (-)^{\mathbf{r}} \kappa_{\mathbf{r}}^z \right|^2 \right\rangle - \left\langle \left| \sum_{\mathbf{r}} (-)^{\mathbf{r}} \kappa_{\mathbf{r}}^z \right| \right\rangle^2 \right]. \quad (7)$$

On the other hand, the sublattice in-plane spin susceptibility was computed as the average of the sublattice squared magnetization,

$$\chi = \frac{1}{2} \sum_{\alpha=x,y} \frac{1}{N} \sum_{\Lambda=A,B,C} \left\langle \left( \sum_{\mathbf{i} \in \Lambda} s_{\mathbf{i}}^{\alpha} \right)^2 \right\rangle, \quad (8)$$

since the average magnetization in the thermodynamic limit is 0. Such a definition retains its value in investigating the divergence of  $\chi$  also for finite lattice simulations, because, even if different from 0, the missing term in Eq. (8) is well behaved and negligible in the critical region. Alternatively, the same information can be also obtained from the total  $\mathbf{k}$ -dependent susceptibility,

$$\chi(\mathbf{k}) = \frac{1}{2} \sum_{\alpha=x,y} \frac{1}{N} \left\langle \left| \sum_{\mathbf{i}} s_{\mathbf{i}}^{\alpha} e^{i\mathbf{k} \cdot \mathbf{i}} \right|^2 \right\rangle, \quad (9)$$

taken at the ordering wavevector  $\mathbf{K}$ , i.e., one of the six vectors pointing towards the corners of the first Brillouin zone of the whole lattice; for example  $\mathbf{K} = (4\pi/3, 0)$ . A straightforward calculation shows indeed that the sublattice susceptibility, defined in Eq. (8), and the total one satisfy the following relation

$$\chi(\mathbf{K}) = \frac{3}{2} \chi - \frac{1}{2} \chi(\mathbf{k}=0), \quad (10)$$

where  $\chi(\mathbf{k}=0)$  is 0 at  $t = 0$ , and is small with respect to the first, also near to the critical point.

The spin correlation length is defined assuming the asymptotic exponential decay form of the in-plane spin correlation functions,

$$C(\mathbf{n}) = \langle s_{\mathbf{i}}^x s_{\mathbf{i}+\mathbf{n}}^x + s_{\mathbf{i}}^y s_{\mathbf{i}+\mathbf{n}}^y \rangle \propto e^{-n/\xi}, \quad (11)$$

with  $\mathbf{i}$  and  $\mathbf{i} + \mathbf{n}$  belonging to the same sublattice, and large values of  $\mathbf{n}$ . Even if a direct fit of the two-point correlation function (11) can be used, we adopted a faster and more reliable method to evaluate  $\xi$ . This can be achieved translating Eq. (11) in the reciprocal space. In fact, the asymptotic exponential decay in real space is associated with the Ornstein-Zernicke form of the Fourier transform of the (full lattice) spin correlation function, i.e., the  $\mathbf{k}$ -dependent susceptibility  $\chi(\mathbf{k})$ , behaving as

$$\chi(\mathbf{K}+\mathbf{k}) \propto \frac{1}{k^2 + \xi^{-2}}, \quad (12)$$

for small values of the wave vector  $\mathbf{k}$ . Since the first Brillouin zone of the finite lattice is discrete, it is not possible to take arbitrarily small values of  $\mathbf{k}$ : we used a fit with the first four shells around  $\mathbf{k} = 0$ . An alternative way we used was to extract the value of  $\xi$  using just the smallest available  $\mathbf{k}$ :

$$\xi = \frac{1}{k_1} \left[ \frac{\chi(\mathbf{K})}{\chi(\mathbf{K}+\mathbf{k}_1)} - 1 \right]^{1/2}, \quad (13)$$

with, e.g.,  $\mathbf{k}_1 = (0, 4\pi/L\sqrt{3})$ .

## IV. RESULTS AND COMMENTS

### A. Thermodynamic behaviour

We performed simulations on the XXZ model for values of  $\lambda = 0, 0.5, 0.9, 0.99$ , ranging from the strongest easy-plane anisotropic case to the quasi-Heisenberg case. The isotropic model was also considered not only to compare the results of our simulation code with the data reported in the literature<sup>1,2,3</sup> but also to check the consistency of the quasi-Heisenberg limit.

The internal energy per spin  $e$  for the XXZ model with  $\lambda = 0$ , is reported in Fig. 2 as a function of the reduced temperature  $t$ . For comparison, data for the XY model taken from Ref. 4 and for the isotropic model are also shown. It is evident from the figure that the qualitative

behaviour of the internal energy is quite different in the isotropic and planar cases. In fact in the latter cases the internal energy presents a narrow region in which size-dependence is apparent, and the slope becomes steeper the larger the lattice size. Instead, the behaviour of the same quantity in the isotropic case is smoother and only with a weak size dependence (not shown in the figure). In the low temperature region the internal energy, according to the spin wave approximation and the equipartition theorem, is linear in  $t$ . While in the XY model the internal energy starts from the ground state value  $e_0 = -3/2$  with slope  $1/2$ , in the other two cases the slope is  $1$ , because of the different number of degrees of freedom: one per spin in the former, two in the latter cases. Increasing the temperature, the excitation of the out-of-plane component of the spins becomes more and more important and causes the different behaviour between the isotropic and XX0 case. Similar behaviour is observed for all the values of  $\lambda \neq 0$  considered.

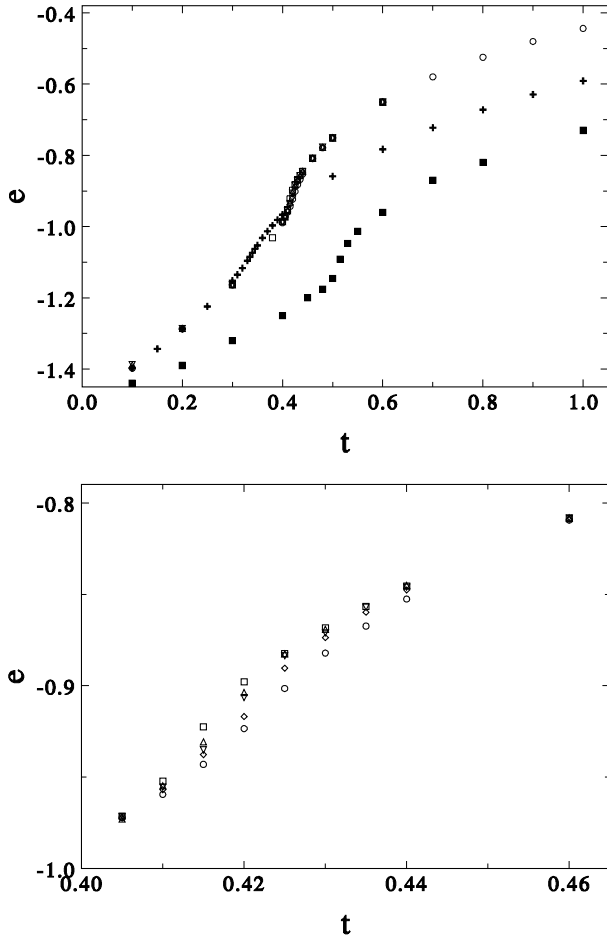


FIG. 2. Internal energy for the XX0 model for lattice sizes  $L = 24$  (circles),  $L = 36$  (diamonds),  $L = 48$  (down triangles),  $L = 60$  (up triangles) and  $L = 120$  (squares). Data for the XY model with  $L = 30$ , taken from Ref. 4 (full squares), and for the isotropic case with  $L = 60$  (crosses) are also shown for comparison. In the lower figure the data are reported in a magnified scale in order to emphasize the size-dependence.

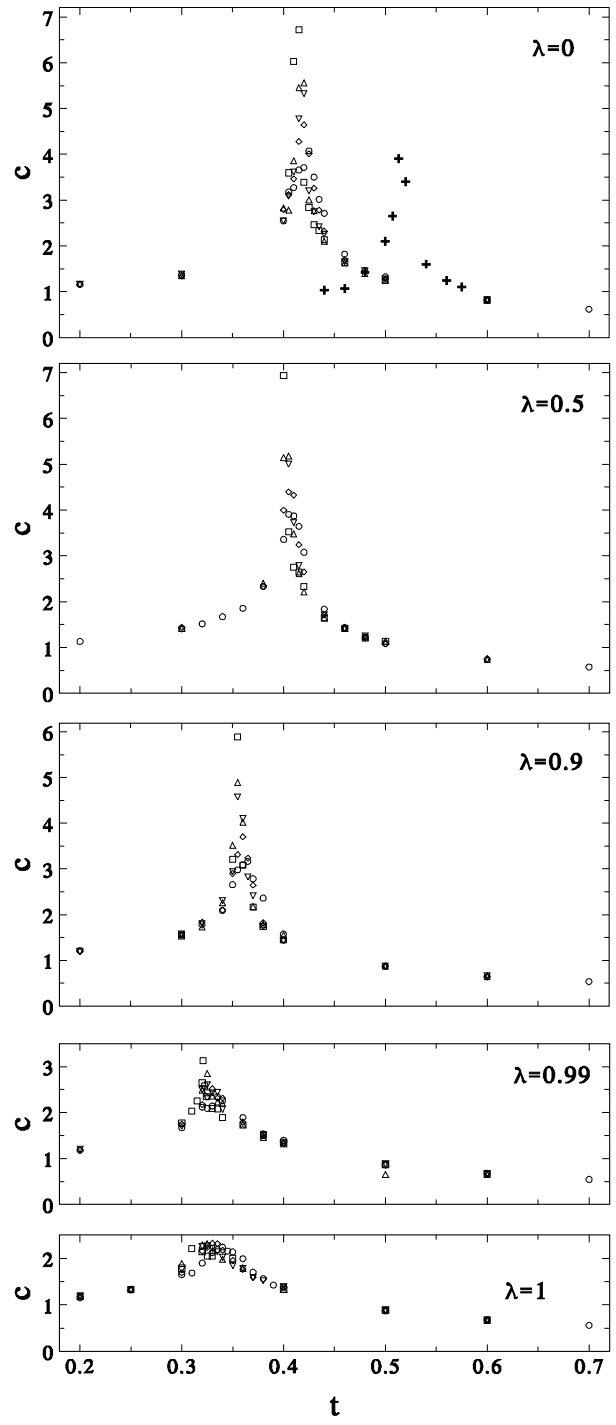


FIG. 3. Specific heat for the XXZ model for the reported values of  $\lambda$  and different values of  $L$ . In the top graph the specific heat observed in the XY model, for  $L = 72$ , taken from Ref. 5, is also shown (crosses). Open symbols as in Fig. 2.

The specific heat data are reported in Fig. 3 for all the values of  $\lambda$  (including the isotropic case). For  $\lambda \neq 1$  the specific heat shows the signature of a divergence which is an important feature of the frustrated planar antiferromagnet, also present in the XY case (the corresponding peak, taken from Ref. 5, is shown in the figure on the

top). As  $\lambda \rightarrow 1$  the peak and the size dependence of its height become less and less pronounced, until, in the isotropic limit, no divergence at all is observed. The size dependence of the peak height is shown in Fig. 4, for  $\lambda = 0, 0.9$  and  $0.99$ . It suggests a logarithmic divergence with  $L$ , just as in the two-dimensional Ising model<sup>24</sup>.

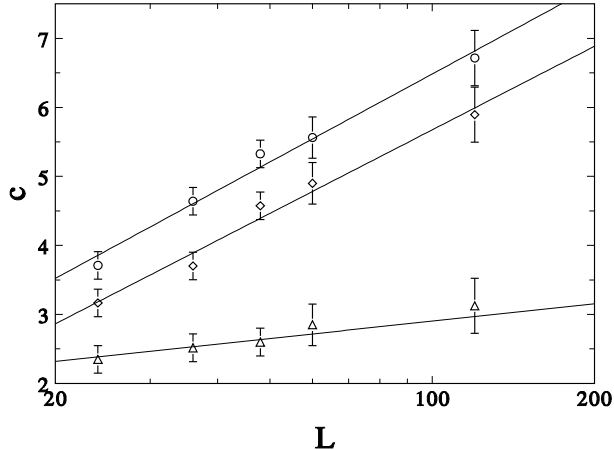


FIG. 4. Maximum of the specific heat as a function of  $L$  for  $\lambda = 0$  (circles),  $0.9$  (diamonds) and  $0.99$  (triangles). The straight lines are guides for the eye.

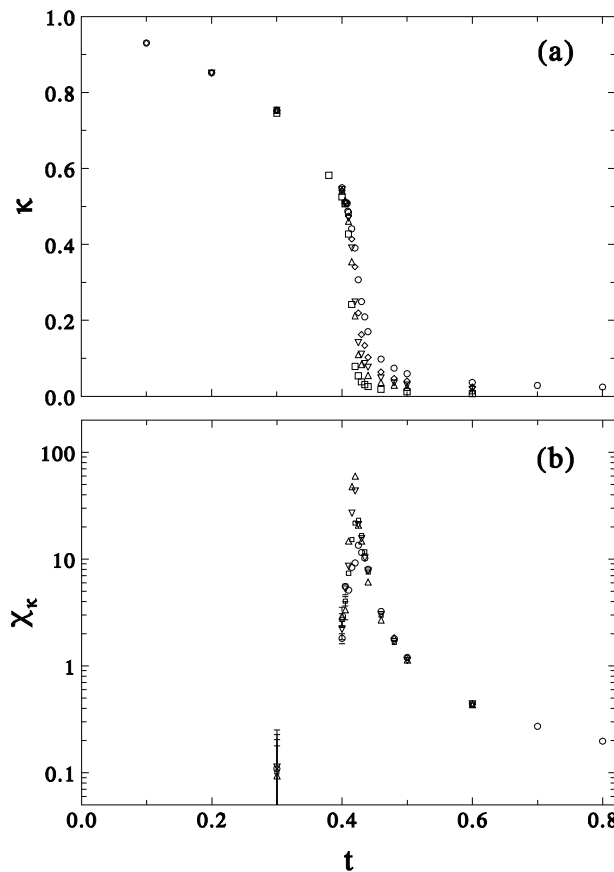


FIG. 5. Staggered chirality (a) and chiral susceptibility (b) for  $\lambda = 0$  and various values of  $L$ , as functions of temperature. Symbols as in Fig. 2.

The critical behaviour associated with the order-disorder transition can be also observed in the staggered chirality and in its susceptibility, defined in Eqs. (5), (6), and (7), and shown in Fig. 5 for  $\lambda = 0$ . At quite low temperatures the system displays chirality order, witnessed by the high value of  $\kappa$ . As the temperature raises, the number of cells with small chirality increases, and domains with opposite staggered chirality develop in the lattice. This leads to a sharp drop of the chirality and to the divergence of the chiral susceptibility at  $t_c \simeq 0.41$ .

The transition is also shown by the behaviour of the correlation function of the staggered chirality, namely

$$C_\kappa(\mathbf{R}) = \langle (-)^{\mathbf{R}} \kappa_{\mathbf{r}}^z \kappa_{\mathbf{r}+\mathbf{R}}^z \rangle, \quad (14)$$

$\mathbf{R}$  being one of the Bravais vectors of the dual lattice. This is shown in Fig. 6 for  $\lambda = 0$ ,  $L = 60$ , and several temperatures. A low temperature phase in which the system is completely correlated is evident for  $t \lesssim 0.42$ . Increasing the temperature, the correlation functions fall off exponentially. Of course it is hard to extract from the correlation functions an accurate estimate of the critical temperature since, approaching  $t_c$  from above, when the correlation length becomes larger than the sampled lattice size, the system behaves as if it were correlated, even if, in the thermodynamic limit, it may be not. However, we can approximatively locate the critical region, for  $\lambda = 0$ , between  $t = 0.4$  and  $t = 0.42$ , consistently with the behaviour of the specific heat, the chirality and its susceptibility.

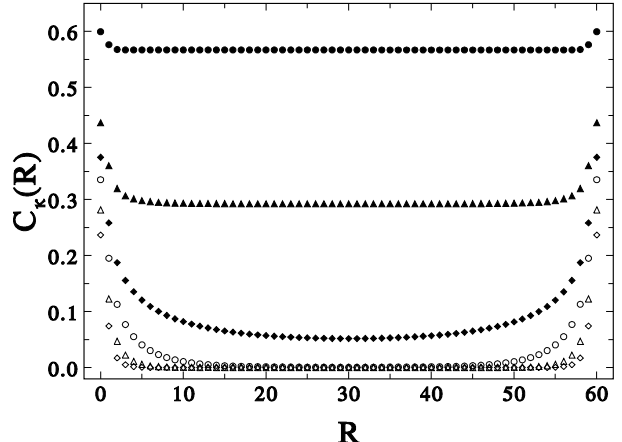


FIG. 6. Chirality correlation function for  $\lambda = 0$ ,  $L = 60$ , and various temperatures:  $t = 0.3$  (full circles),  $t = 0.4$  (full triangles),  $t = 0.42$  (full diamonds),  $t = 0.44$  (circles),  $t = 0.5$  (triangles),  $t = 0.6$  (diamonds).

Let us turn now to the rotational degrees of freedom. We recall that the peculiarities of the BKT transition can be summarized as follows<sup>13,18</sup>. First of all, according to Mermin-Wagner's theorem, the system does not show any finite magnetization in absence of an applied magnetic field, at any  $t \neq 0$  below and above the transition temperature  $t_{\text{BKT}}$ . Although the system cannot display long-range order, below the critical temperature it is characterized by quasi long-range order, whose macro-

scopic consequence is the power-law decay of the correlation functions of the in-plane spin components,

$$C(\mathbf{n}) = \langle s_{\mathbf{i}}^x s_{\mathbf{i}+\mathbf{n}}^x + s_{\mathbf{i}}^y s_{\mathbf{i}+\mathbf{n}}^y \rangle \propto \frac{1}{n^\eta}, \quad (15)$$

where the critical exponent  $\eta$  is a function of temperature and assumes the universal value of  $\eta = 1/4$  at  $t_{\text{BKT}}$ . This quasi long-range order is not destroyed by the excitation of vortex-antivortex pairs until when, raising the temperature, the pairs unbind and the system undergoes a transition to a disordered phase with exponentially decaying correlation functions. The in-plane correlation length and susceptibility both diverge exponentially for  $t \rightarrow t_{\text{BKT}}^+$

$$\xi \propto a_\xi e^{b_\xi(t-t_{\text{BKT}})^{-1/2}}, \quad (16)$$

$$\chi \propto a_\chi e^{b_\chi(t-t_{\text{BKT}})^{-1/2}}, \quad (17)$$

(where  $\chi(\mathbf{K})$  can also be taken for  $\chi$ ) and are infinite for  $t \leq t_{\text{BKT}}$ . These properties have been also observed in the XY TAF<sup>4,5</sup>, which shares a similar low-temperature phase with the ferromagnetic counterpart, if the sublattice magnetization of the former replaces the uniform magnetization of the latter; for example, the low-temperature phase is well described by Eq. (15), where  $\mathbf{i}$  and  $\mathbf{i} + \mathbf{n}$  belong to the same sublattice.

Another important property of the BKT transition in unfrustrated planar systems is the behaviour of the specific heat, which displays a maximum slightly above the transition temperature (usually at  $t \simeq 1.1 \div 1.2 t_{\text{BKT}}$ <sup>18</sup>). However this maximum cannot be observed in frustrated planar systems<sup>4,5</sup>, where it is hidden by the divergence connected with the chirality transition.

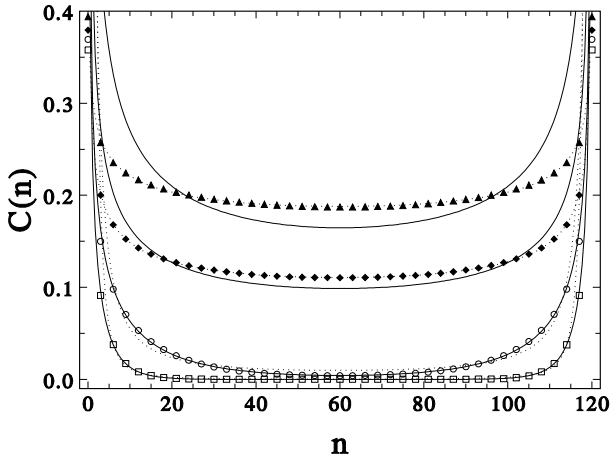


FIG. 7. Spin correlation function for  $\lambda = 0.9$ ,  $L = 120$  and different temperatures:  $t = 0.32$  (full triangles),  $t = 0.35$  (full diamonds),  $t = 0.36$  (circles), and  $t = 0.40$  (squares). Lines are best fits against Eq. (15) (dashed lines) and Eq. (11) (full lines). All fitting functions were properly symmetrized to take into account the periodic boundary conditions applied to the simulated finite-size lattice.

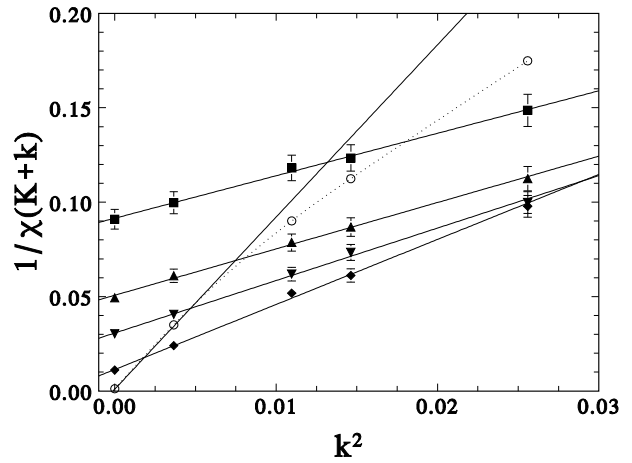


FIG. 8.  $\chi(\mathbf{K}+\mathbf{k})^{-1}$  against  $k^2$ , for  $\lambda = 0.9$  and  $L = 120$ , at different temperatures:  $t = 0.35$  (open circles),  $0.36$  (diamonds),  $0.37$  (down triangles),  $0.38$  (up triangles), and  $0.40$  (squares). The maximum value of  $k^2$ , for the chosen set of wave vector shells, is  $(4\pi/\sqrt{3})^2 \times (7/L^2) \simeq 0.0256$ , so that a linear behaviour (full lines) against  $k^2$  is expected until  $\xi^2(t) \ll 1/0.0256 \simeq 39$ . Indeed, this is not the case for  $t = 0.35$ , when  $\xi \simeq 90$  and the linear fit fails. The dashed line is a guide for the eye.

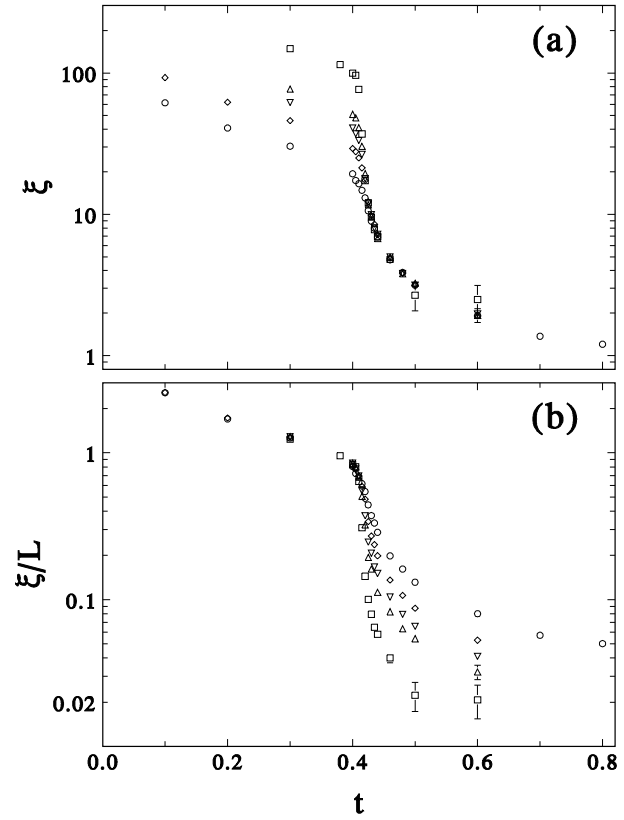


FIG. 9. In-plane correlation length  $\xi$  (a) for the XX0 model as a function of temperature, for different simulation box sizes. In figure (b)  $\xi/L$  is reported to show the finite-size scaling below  $t_{\text{BKT}}$ . Symbols as in Fig. 2.

Fig. 7 displays the correlation functions of the in-plane spin components  $C(\mathbf{n})$  for  $\lambda = 0.9$  and various temperatures, for  $L = 120$ . Fittings against Eq. (15) and Eq. (11) are also shown in the figure. The data for  $t = 0.32$  and  $t = 0.35$  can be fitted only by the power law, while for  $t = 0.36$  and  $t = 0.4$  the exponential decay fits best: given the rather large lattice size, it can be reasonably argued that the critical temperature  $t_{\text{BKT}}(\lambda=0.9)$  is located in between between  $t = 0.35$  and  $t = 0.36$ . As already noticed, it is difficult to extract accurate informations about  $t_{\text{BKT}}$  from the correlation functions since it is not possible to discriminate between the high- and low-temperature predicted behaviour unless data for lattice sizes  $L > \xi$  are available, requirement which cannot be achieved close to the critical temperature.

As already said the methods we used to extract the value of the correlation length  $\xi$  were the fit, according to Eq. (12), of the total in-plane  $\mathbf{k}$ -dependent susceptibility  $\chi(\mathbf{k})$ , around one of the ordering wave vectors  $\mathbf{K}$ , or, alternatively, the use of Eq. (13). We remind that the correlation length of the infinite system (above  $t_{\text{BKT}}$ ) is well defined by Eq. (11); for a finite system, the same is still true for temperatures and lattice sizes large enough that the finite-size effects are negligible; otherwise Eq. (13) can be considered an *ad hoc* definition of  $\xi$ . Provided that  $\xi \lesssim L/6$ , the values of correlation length we got by the two methods were the same within the uncertainties. When finite-size effects become relevant, the results differ from each other of about 4-8%; the first method being less reliable since Eq. (12) is valid for  $\xi^{-2}k^2 \ll 1$ , a condition which cannot be satisfied beyond the wave vectors closest to  $\mathbf{K}$ , as it can be seen in Fig. 8: the values of  $\xi$  reported in Fig. 9, for  $\lambda = 0$ , are those obtained in the second way. The correlation length below  $t_{\text{BKT}}$ , as well as in a neighbourhood above it, has been evaluated just to check where finite-size effects become relevant and in order to verify the finite-size scaling law  $\xi \propto L$ .

Fig. 10 shows the in-plane ( $\chi$ ) and out-of-plane ( $\chi^{zz}$ ) sublattice susceptibilities, defined in Eq. (8), as functions of temperature, for different values of  $\lambda$  and of the lattice sizes. As expected, the susceptibility displays finite size-effects like the correlation length and the rule of thumb  $\xi \lesssim L/6$ , for neglecting such effects also applies. The behaviour of the out-of-plane sublattice susceptibility  $\chi^{zz}$ , shown in the same figure, is also an interesting feature of the BKT transition, also present in the XXZ model on bipartite lattice<sup>18</sup>, which, of course, has no counterpart in the XY models. As expected, the absolute magnitude of  $\chi^{zz}$  increases, as lambda increases, the system becoming more isotropic and the out-of-plane fluctuations becoming easier. However, for every value of  $\lambda \neq 1$ , the easy-plane character of the system prevails at low temperatures and for  $t \rightarrow 0$ ,  $\chi^{zz} \rightarrow 0$ ; on the other hand, in the opposite limit, the effects of the anisotropy of the interactions disappear, all spins can fluctuate independently from each other and both the in-plane and out-of-plane susceptibilities approach the common value  $1/3$ . Starting from the high temperature limit, and coming to lower temperatures,  $\chi$  increases whatever the value of

$\lambda \neq 1$  is, ending to diverge at  $t_{\text{BKT}}$ ; of course, the smaller is the anisotropy, the longer  $\chi^{zz}$  follows the behaviour of  $\chi$ . The result is that, as  $\lambda \rightarrow 1$ ,  $\chi^{zz}$  develops a sharper and sharper maximum.

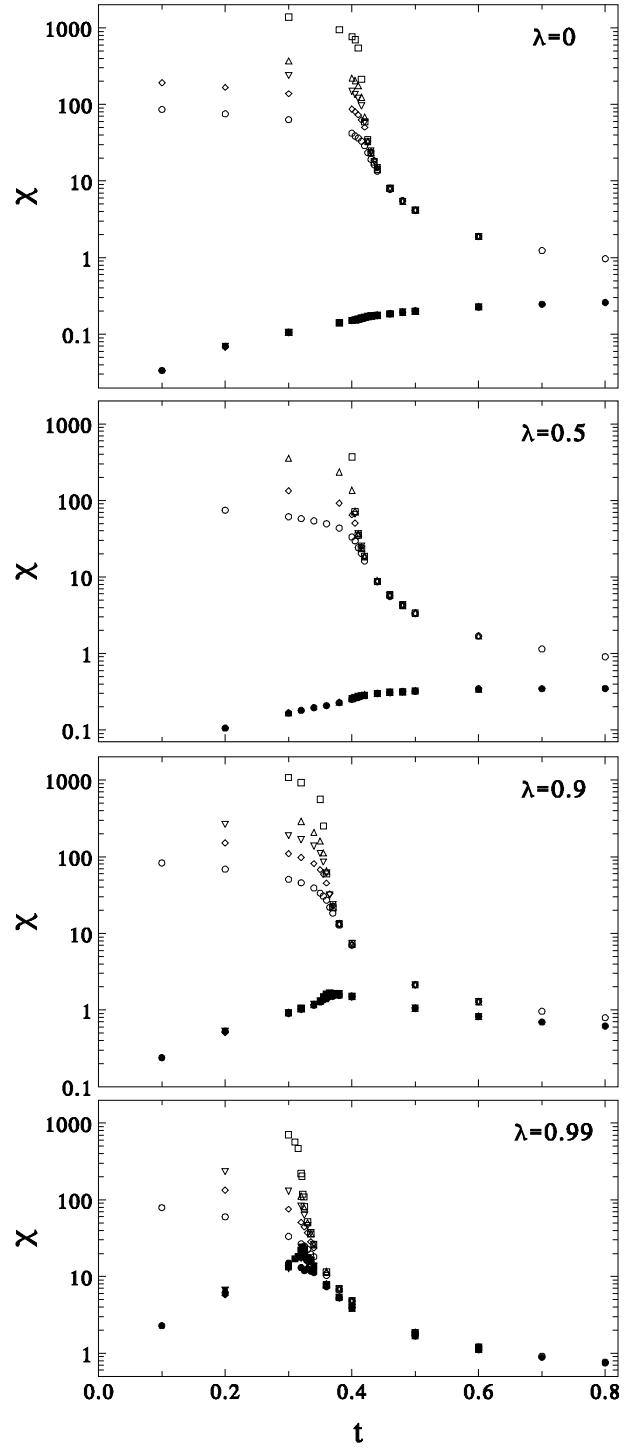


FIG. 10. In-plane (open symbols) and out-of-plane (full symbols) susceptibilities as functions of temperature, for the values of  $\lambda$  reported in each figure. Different symbols refer to the simulation box sizes as in Fig. 2.

## B. Critical temperatures

### 1. Order-disorder transition

As we have seen in the previous sections the behaviour of the specific heat, chirality and its susceptibility as functions of temperature indicates the presence of an Ising-like phase transition connected with the loss of the chirality order for every value of  $\lambda < 1$  considered. Those thermodynamic quantities allow us to estimate immediately, at least approximately, the corresponding critical temperatures,  $t_c$ , since the transition appears rather sharp for all the values of  $\lambda$ . A finite-size scaling analysis of these data shows that the features of such phase-transition are consistent with two-dimensional Ising exponents.

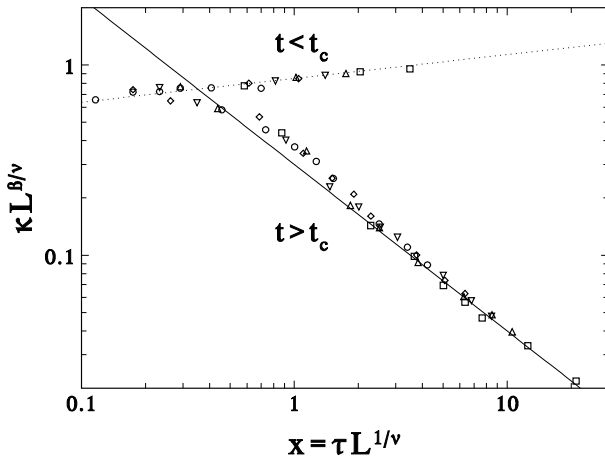


FIG. 11. Finite-size scaling analysis for the staggered chirality  $\kappa$ , for  $\lambda = 0$ . Ising exponents  $\beta = 1/8$  and  $\nu = 1$  are used. Different symbols refer to the simulation box sizes as in Fig. 2.

In Fig. 11  $\kappa L^{\beta/\nu}$  is reported, for  $\lambda = 0$  and  $t_c = 0.412$ , as a function of the reduced variable  $x = \tau L^{1/\nu}$ ; where  $\tau$  is  $1 - t/t_c$  for  $t < t_c$  and  $1 - t_c/t$  otherwise<sup>5,25</sup>. According to the scaling-hypothesis, close to the infinite lattice  $t_c$  the order parameter  $\kappa$  is given by

$$\kappa = L^{-\beta/\nu} f(x), \quad (18)$$

where, since for  $L \rightarrow \infty$  the power-law singularities are to be reproduced, the limiting form of the function  $f(x)$  for  $x \rightarrow \infty$  and  $t < t_c$  is

$$f(x) \propto x^\beta. \quad (19)$$

Therefore, reporting as in Fig. 11  $\kappa L^{\beta/\nu}$  versus  $x$ , the data for the various lattice sizes do collapse onto a single curve, which is of course  $f(x)$  if the values of  $t_c$ ,  $\beta$ , and  $\nu$  are correct. In the present case using the critical exponents of the two-dimensional Ising model,  $\nu = 1$  and  $\beta = 1/8$ , a good agreement with the finite-size scaling law is obtained. Below  $t_c$  the large- $x$  behaviour reproduces the correct critical behaviour, which, in a double-logarithmic scale, is represented by a line with slope

$\beta = 1/8$ . Above  $t_c$  the asymptotic behaviour shows the  $1/L$  decay of the order parameter<sup>25</sup> as  $L \rightarrow \infty$  which means, according to Eq. (18),  $f(x) \propto x^{\beta-1}$ . This corresponds to the line with slope  $-7/8$  in the figure. In this way it has been possible to give the estimates of the critical temperature reported in Table I.

### 2. BKT transition

In order to estimate the critical temperature associated with the BKT transition we relied on two methods: firstly, the fit of the correlation length and the in-plane susceptibility with Eqs. (16) and (17), using the MC data that are representative for their thermodynamic limit, i.e., for  $t \gtrsim t_{\text{BKT}}$ ; secondly, we used the finite-size scaling law

$$\chi \propto L^{2-\eta(t)}, \quad (20)$$

which is valid for  $t \lesssim t_{\text{BKT}}$ , to obtain the scaling exponent  $\eta(t)$ , that satisfies  $\eta(t_{\text{BKT}}) = 1/4$ . Noteworthy, the latter method makes use of a different and independent data set.

As for the first method, we have tested for BKT behaviour, i.e., with Eqs. (16) and (17), both the correlation length  $\xi(t)$  and the susceptibility  $\chi(t)$ . As said above, in doing this only the reliable estimates of the thermodynamic limit of these quantities were kept, after the criterion  $\xi(t) \lesssim 6L$ , in order to discard the data affected by finite-size effects. Of course, this has prevented us from obtaining useful estimates  $\xi(t)$  and  $\chi(t)$  for  $t$  close to the transition temperature, due to the large computer-time required to simulate large systems. Indeed, when simulating a larger lattice, besides the increase of the time needed for any move ( $\propto N = L^2$ ), we must also face the increase of MC fluctuations and correlation time, so that much more sample configurations should be generated in order to keep uncertainties at a reasonable level. This would imply resorting to large-scale simulations which is well beyond our purposes. The results for the BKT transition temperatures from the fits of the representative data are summarized in Table II; since  $\chi(t)$  is a direct outcome of the MC simulation, its values and the consequently fitted values of  $t_{\text{BKT}}$  are more accurate than those for  $\xi(t)$ , which must indeed be derived by fitting the MC outcomes for the  $\mathbf{k}$ -dependent susceptibility. The uncertainties account both for the statistical error and for the instability of the fit against exclusion of the data points at the lowest temperature, where  $\xi(t) \sim L/6$ .

As for the use of Eq. (20), in actual numerical calculations it holds also slightly above  $t_{\text{BKT}}$ , when  $L$  is still smaller than the thermodynamic  $\xi$  and the system is already correlated. In fact this scaling relation allows us to give an estimate of the parameter  $\eta(t)$  and, by looking at which temperature such quantity attains the value  $1/4$ , to have an independent check of the estimated critical temperature. In Fig. 12,  $\chi/L^{7/4}$  is plotted on a doubly logarithmic scale as a function of the lattice size  $L$  for  $\lambda = 0.50$ . The data fall clearly on a straight line for

$t \leq 0.40$ , the slope of the lines being the corresponding values of  $1/4 - \eta$ ; they already depart from linearity, instead, for  $t = 0.41$ . The values for the quantity  $1/4 - \eta$  we obtain by fitting the susceptibility data with Eq. (20) are reported, for the various values of  $\lambda$  considered, in Table III. By interpolation, the values of  $t_{\text{BKT}}$  appearing in the fourth column can be computed. These data agree reasonably well with those obtained by fitting  $\xi$  and  $\chi$  with Eqs. (16) and Eqs. (17), shown in Table II; the trend to a slight overestimation of  $t_{\text{BKT}}$  for the higher values of  $\lambda$  was already observed for the square-lattice case in Ref. 18.

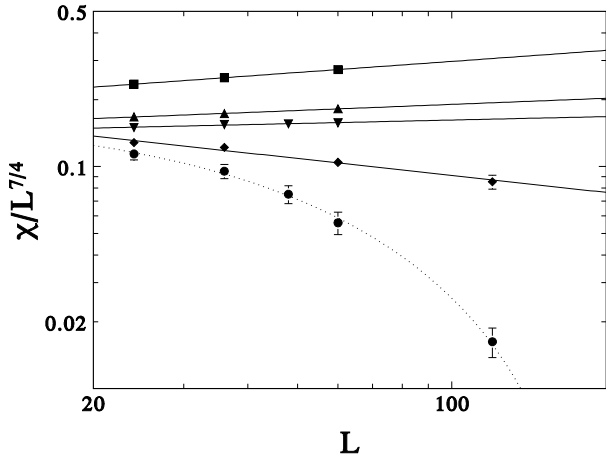


FIG. 12. In-plane susceptibility over  $L^{7/4}$  vs  $L$ , for  $\lambda = 0.5$ , at different temperatures around the critical one:  $t = 0.30$  (squares), 0.38 (up triangles), 0.39 (down triangles), 0.40 (diamonds), and 0.41 (circles).

For every value of  $\lambda$  the critical temperature  $t_c$  is significantly higher than the BKT transition temperature  $t_{\text{BKT}}$ , although their difference is not much larger than the uncertainties. Also in this respect the situation is to that of the XY TAF, where there is no agreement in the literature on whether a single or a double phase-transition takes place. Nevertheless, the fact that  $t_c \gtrsim t_{\text{BKT}}$  for all values of  $\lambda$  in a systematic way, makes it unlikely that the difference could just be due to statistical errors.

## V. CONCLUDING REMARKS

We have performed Monte Carlo simulations of the two-dimensional XXZ model on a triangular lattice at different values of the easy-plane anisotropy constant  $\lambda$ . For every value of  $\lambda$  considered, the situation appears quite similar to that observed in the XY triangular anti-ferromagnet, where frustration induces an order-disorder transition, associated with the two-fold additional degeneracy of the ground state, and a BKT transition connected with the sublattice in-plane orientational ordering. The critical behaviour turns out to be consistent with an Ising transition, for the internal energy, specific heat, chirality and the associated susceptibility, while

it is consistent with a BKT transition with respect to the in-plane correlation length and susceptibility. The value of both the critical temperatures decreases with anisotropy strength, as shown in Fig. 13; this is consistent with the fact that the critical behaviour observed is connected with the planar character of the system, and that both the chirality and the orientational quasi-ordering are disturbed by the out-of-plane fluctuations of the spins which, at a fixed temperature, increase with the value of  $\lambda$ . For the same reason the phase transition in the XX0 model takes place at a temperature ( $t \simeq 0.403$ ) which is sensibly lower than that observed in the XY model ( $t \simeq 0.505$ ), where the spins are confined in the  $xy$  plane. As for the question of whether a single or two phase transitions are occurring, our results for the transition temperatures (Fig. 13) support the second hypothesis, consistently also with the most recent high-precision MC simulations of the fully frustrated XY model<sup>7</sup>, where the existence of a new universality class is ruled out.

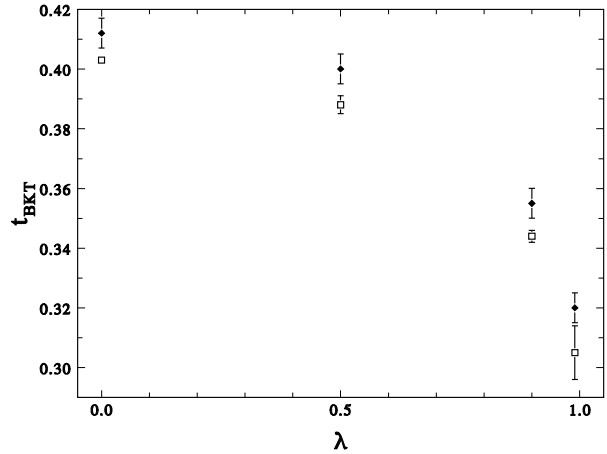


FIG. 13. Transition temperatures for the Ising-like transition (full diamonds) and for the BKT one (squares), the latter estimated through the BKT fit of the susceptibility, vs. the anisotropy.

TABLE I. Critical temperature  $t_c$  associated to the chirality phase-transition.

$\lambda$	$t_c$
0.00	$0.412 \pm 0.005$
0.50	$0.400 \pm 0.005$
0.90	$0.355 \pm 0.005$
0.99	$0.320 \pm 0.005$

\* Present address: Scuola Internazionale Superiore di Studi Avanzati, Via Beirut 2-4, 34013 Trieste, Italy. Electronic address: capriotti@fi.infn.it, caprio@sissa.it

† Electronic address: vaia@ieq.fi.cnr.it

‡ Electronic address: cuccoli@fi.infn.it

§ Electronic address: tognetti@fi.infn.it

<sup>1</sup> H. Kawamura and S. Miyashita, J. Phys. Soc. Jpn. **53**, 4138 (1984).

<sup>2</sup> P. Azaria, B. Delanotte, and D. Mouhanna, Phys. Rev. Lett. **68**, 1762 (1992).

<sup>3</sup> M. Wintel, H. U. Everts, and W. Apel, Phys. Rev. B **52**, 13480 (1995).

<sup>4</sup> S. Miyashita and H. Shiba, J. Phys. Soc. Jpn. **53**, 1145 (1984).

<sup>5</sup> D. H. Lee, J. D. Joannopoulos, J. W. Negele, and D. P. Landau, Phys. Rev. Lett. **52**, 433 (1984); Phys. Rev. B **33**, 450 (1986).

<sup>6</sup> S. Teitel and C. Jayaprakash, Phys. Rev. B **27**, 598 (1983).

<sup>7</sup> P. Olsson, Phys. Rev. Lett. **75**, 2758 (1995) and **77**, 4850 (1997); Phys. Rev. B **55**, 3585 (1997).

<sup>8</sup> A. Cuccoli, R. Giachetti, V. Tognetti, P. Verrucchi, and R. Vaia, J. Phys.: Condens. Matter **7**, 7891 (1995).

<sup>9</sup> C. Biagini, A. Cuccoli, V. Tognetti, P. Verrucchi, R. Vaia, J. Appl. Phys. **79**, 4638 (1996).

<sup>10</sup> A. Cuccoli, V. Tognetti, P. Verrucchi, and R. Vaia, Phys. Rev. Lett. **77**, 3439 (1996), and **79**, 1584 (1997).

<sup>11</sup> L. Capriotti, A. Cuccoli, V. Tognetti, R. Vaia, and P. Verrucchi, Physica D (in press, 1997).

<sup>12</sup> N. D. Mermin and H. Wagner, Phys. Rev. Lett. **17**, 1133 (1966).

<sup>13</sup> V. L. Berezinskii, Zh. Eksp. Teor. Fiz. **59**, 907 (1970); J. M. Kosterlitz and D. J. Thouless, J. Phys. C **6**, 1181 (1973); J. M. Kosterlitz, J. Phys. C **7**, 1046 (1974).

<sup>14</sup> G. H. Wannier, Phys. Rev. **79**, 357 (1950).

<sup>15</sup> R. A. Pelcovits and D. R. Nelson, Phys. Lett. **57 A**, 23 (1976)

<sup>16</sup> S. B. Khokhlov, Zh. Eksp. Theor. Fiz. **70**, 265 (1976).

<sup>17</sup> S. Hikami and T. Tsuneto, Prog. Theor. Phys. **63**, 387 (1980).

<sup>18</sup> A. Cuccoli and V. Tognetti, R. Vaia, Phys. Rev. B **52**, 10221 (1995).

<sup>19</sup> G. M. Wysin, Phys. Rev. B **49**, 8780 (1994).

<sup>20</sup> N. Metropolis *et al.* J. Chem. Phys. **21** 1087 (1953).

<sup>21</sup> F. R. Brown and T. J. Woch, Phys. Rev. Lett. **58**, 2394 (1987).

<sup>22</sup> M. Creutz, Phys. Rev. D **36**, 515 (1987).

<sup>23</sup> N. Madras and A. D. Sokal, J. Stat. Phys. **50**, 109 (1988).

<sup>24</sup> M. N. Barber, in *Phase Transitions and Critical Phenomena*, edited by C. Domb and J. L. Lebowitz (Academic, London, 1983), Vol. 8, pp. 145-266.

<sup>25</sup> D. P. Landau, Phys. Rev. B, **13**, 2997 (1976).

TABLE II. BKT transition temperature as obtained fitting the in-plane correlation length  $\xi(t)$  and the in-plane susceptibility  $\chi$  against Eqs. (16) and (17).

$\lambda$	$t_{\text{BKT}}$ ( $\xi$ fit)	$t_{\text{BKT}}$ ( $\chi$ fit)
0.00	$0.402 \pm 0.002$	$0.403 \pm 0.001$
0.50	$0.391 \pm 0.002$	$0.388 \pm 0.003$
0.90	$0.345 \pm 0.006$	$0.344 \pm 0.002$
0.99	$0.306 \pm 0.008$	$0.305 \pm 0.009$

TABLE III. Scaling exponent  $\eta(t)$  as obtained by direct finite-size scaling analysis of the in-plane susceptibility data according to Eq. (20). The values of  $t_{\text{BKT}}$  given in the fourth column are obtained by interpolation of the function  $\eta(t)$  at the point  $\eta = 1/4$ .

$\lambda$	$t$	$1/4 - \eta$	$t_{\text{BKT}}$
0.00	0.300	$0.165 \pm 0.002$	
	0.400	$0.054 \pm 0.005$	
	0.405	$0.051 \pm 0.007$	
	0.410	$-0.06 \pm 0.01$	$0.407 \pm 0.003$
	0.300	$0.1654 \pm 0.0007$	
	0.380	$0.09 \pm 0.04$	
	0.390	$0.052 \pm 0.008$	
	0.400	$-0.25 \pm 0.03$	$0.391 \pm 0.005$
	0.300	$0.1486 \pm 0.0005$	
	0.320	$0.13 \pm 0.06$	
0.50	0.340	$0.068 \pm 0.008$	
	0.350	$0.00 \pm 0.01$	$0.350 \pm 0.005$
	0.200	$0.204 \pm 0.009$	
	0.300	$0.131 \pm 0.02$	
	0.310	$0.08 \pm 0.01$	
	0.315	$-0.02 \pm 0.01$	$0.314 \pm 0.002$